ACS OMEGA

http://pubs.acs.org/journal/acsodf

Article

Induction Heating Analysis of Surface-Functionalized Nanoscale $CoFe_2O_4$ for Magnetic Fluid Hyperthermia toward Noninvasive Cancer Treatment

Prashant B. Kharat,* Sandeep B. Somvanshi,* Pankaj P. Khirade,* and K. M. Jadhav*

Cite This: *ACS Omega* 2020, 5, 23378−23384

Read Online

ACCESS | Metrics & More | Article Recommendations

ABSTRACT: Oleic acid-coated cobalt ferrite nanoparticles were synthesized using the chemical co-precipitation route and characterized by standard techniques for structure, morphology, and magnetic properties analysis. The Rietveld refined X-ray diffraction (XRD) pattern of $CoFe_2O_4$ nanoparticles indicated the formation of a cubic-spinel single-phase structure with the $Fd\bar{3}m$ space group. The average crystallite size (∼12 nm) confirmed the nanocrystalline appearance of the prepared $CoFe_2O_4$ nanoparticles. Transmission electron microscopy (TEM) images revealed the spherical nature of both ($CoFe_2O_4$) and (OA-$CoFe_2O_4$) samples. The absorption bands in the Fourier transform infrared (FT-IR) spectrum at ∼3418, 3026, 1628, 1404, 1068, 845, 544, and 363 cm^{-1} affirmed the spinel ferrite formation and OA attachment. The M−H curve recorded at room temperature showed the superparamagnetic nature of the $CoFe_2O_4$ nanoparticles with moderate saturation magnetization (∼78 emu/gm). The blocking temperature of the prepared $CoFe_2O_4$ nanoparticles obtained from the field-cooled and zero-field-cooled (FC−ZFC) curve was estimated to be 144 K. Further, the characterized surface-modified $CoFe_2O_4$ was then added in ethylene glycol/water with various concentrations and characterized by the induction heating technique for the evaluation of their self-heating characteristics. A series of temperature versus time measurements were made by varying the ethylene glycol/water proportion for better understanding of the self-heating characteristics of the prepared $CoFe_2O_4$ nanoparticles. All of the findings display the applicability of the surface-modified $CoFe_2O_4$ nanoparticles in magnetic fluid hyperthermia toward noninvasive cancer treatment and other bio-applications.

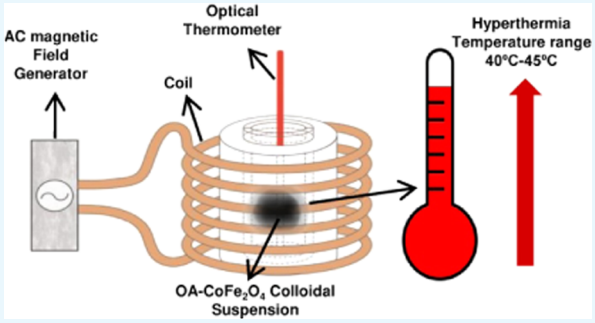

1. INTRODUCTION

Magnetic nanomaterials with appropriate physicochemical properties, functionalized surface, and improved biocompatibility have been broadly examined for different restorative, indicative, and remedial applications, for example, specific drug delivery, fluid hyperthermia, as a contrast enhancer in magnetic resonance or reverberation imaging (MRI), cell detachment, tissue fixing, biosensors, and so forth.[1−6] The physicochemical properties, colloidal strength, and biocompatibility of these magnetic nanomaterials can be vitally constrained by precise synthesis conditions and functionalization of the surface. Magnetic platforms with nanometric size (of the order of a few nanometers) and thin size distribution with upgraded magnetic properties comprise the prime necessity for biomedical application purposes. Likewise, magnetic nanoparticles should also have consolidated high susceptibility for the best magnetic enhancement and quicker loss of magnetization after disposal of the outer guest magnetic field. Magnetic fluid hyperthermia, a modular strategy for disease treatment with the desired temperature, in the range of 41−45 °C, and a treatment period of least 20 min, has been paid great attention to because of its lower clinical symptoms and probability to obliterate particular territory of harmful malignancy tumor.[7−9] This procedure includes the consolidation of superparamagnetic or ferromagnetic particles into the dangerous tumor cell and then illumination with a substituting magnetic field.[10]

In previous decades, much research of magnetic nanomaterials for biomedical field (specifically hyperthermia) has been centered on superparamagnetic iron oxide materials, for example, Fe_3O_4 and γ-Fe_2O_3, which show smaller saturation magnetization values.[11−13] In contrast, some transition metals, for example, Ni, Co, and so on, acquire large saturation magnetization values, similarly moderate anisotropy, steady K_{eff}, and larger losses. Recently, spinel-structured ferrite nanomaterials, a type of general magnetic nanomaterials, have attracted

Received: July 11, 2020
Accepted: August 18, 2020
Published: September 2, 2020

https://dx.doi.org/10.1021/acsomega.0c03332
ACS Omega 2020, 5, 23378−23384

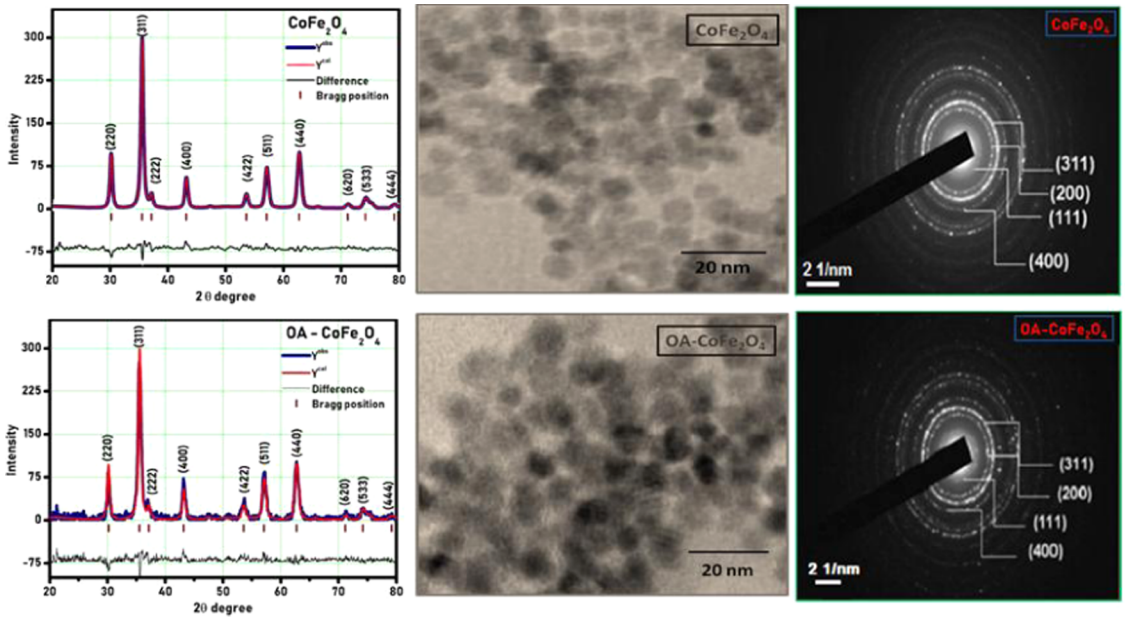

Figure 1. XRD patterns, transmission electron microscopy (TEM) images, and selected area electron diffraction (SAED) patterns of PR-CF and SM-CF nanoparticles.

the great attention of researchers and scientists.[14−18] Spinel ferrite containing $M^{II}Fe_2O_4$ (where M^{II} = Co^{2+}, Ni^{2+}, Zn^{2+}, Mn^{2+}, and so on) shows noteworthy physicochemical properties.[19−24] Among spinel ferrites, cobalt spinel ferrite ($CoFe_2O_4$) is important from the biomedical application perspective because of its great saturation magnetization, high permeability, and no favored direction of magnetization.[25] In addition, it displays high anisotropy of the order 190−280 kJ/m^3 in correlation with alternate ferrites. Hence, the magnetic moment of $CoFe_2O_4$ relaxes with a much slower rate than other iron oxide nanoparticles of same size. This suggests that $CoFe_2O_4$ nanoparticles with a nanometric size range can be utilized as an alternative of iron oxide nanoparticles in hyperthermia applications. Utilization of $CoFe_2O_4$ nanoparticles in the biomedical field is very monotonous due to a few issues, for example, aggregation of nanoparticles in solution and the toxicity of the material. To overcome these issues, coating $CoFe_2O_4$ nanoparticles with suitable surfactants, for example, oleic acid, polyethylene glycol, and so forth, produces a protecting layer and lessens the direct and immediate exposure of the $CoFe_2O_4$ nanoparticles surface to the organic climate. Oleic acid (OA) is one of the promising coating agents having complementary anticancerous and anti-inflammatory behavior.[26] Oleic acid coating helps us to stabilize the nanoparticles in fluidic media and enhances the dispersion stability of the nanoparticles with less agglomeration. Also, oleic acid coating increases the biocompatibility of the nanoparticles, which is one of the main concerns of the biomedical applications of nanoparticles.[27]

In recent decades, surface-functionalized spinel ferrites, especially $CoFe_2O_4$ nanoparticles prepared by utilizing wet chemical techniques were explored by the academic and scientific network for biomedical applications, for example, directed drug loading, magnetic hyperthermia, and magnetic resonance imaging.[28,29] These analyses were fundamentally centered on the inductive heating properties of $CoFe_2O_4$ nanoparticles synthesized by the hydrothermal method and the sol−gel autoburning technique. However, very few reports are available on water-dispersible $CoFe_2O_4$ nanoparticles prepared by the chemical co-precipitation method and functionalized by oleic acid. The $CoFe_2O_4$ nanoparticles are effectively dispersed and stable in combination with water and ethylene glycol in contrast to other fluidic mediums, which results in a superior self-warming at lower attractive field. In correlation with other synthesis routes, the chemical co-precipitation strategy showed numerous advantages, for example, better homogeneity, small particle size, moderately low reaction temperature, thin size distribution, low cost, and so on.[30,31] Thus, herein, we report the synthesis, characterization, and induction heating evaluation of surface-modified $CoFe_2O_4$ nanoparticles co-dispersed in water/ethylene glycol. Oleic acid-coated cobalt ferrite nanoparticles were synthesized using the chemical co-precipitation route and characterized by standard techniques for structure, morphology, and magnetic properties analysis. Further, the characterized surface-modified $CoFe_2O_4$ was then added in ethylene glycol/water with various concentrations and characterized by the induction heating technique for evaluation of their self-heating characteristics. A series of temperature versus time measurements were done by varying the ethylene glycol/water proportion for better understanding of the self-heating characteristics of the prepared $CoFe_2O_4$ nanoparticles.

2. RESULTS AND DISCUSSION

The pristine and surface-modified $CoFe_2O_4$ samples were coded as PR-CF and SM-CF, respectively. The recorded X-ray diffraction (XRD) patterns of PR-CF and SM-CF are shown in Figure 1, which reveals that both the PR-CF and SM-CF samples exhibit good crystalline nature that confirms the formation of a pure-phase nanoparticle without any impurity phase. Rietveld refinement of both the PR-CF and SM-CF samples was done by FullProf Suite software. It is confirmed from Figure 1 that functionalization of the oleic acid on the surface of the $CoFe_2O_4$ nanoparticles did not modify the crystal structure of the PR-CF. A small noise was recorded in the XRD pattern of SM-CF due to the amorphous nature of oleic acid

https://dx.doi.org/10.1021/acsomega.0c03332
ACS Omega 2020, 5, 23378−23384

layer on the surface of the $CoFe_2O_4$ nanoparticles. Table 1 shows the values of structural parameters of PR-CF and SM-CF nanoparticles deduced from XRD data.

Table 1. Values of Lattice Constant (a), Crystallite Size (D), Particle Size (t), X-ray Density (d_X), Bulk Density (d_B), and Porosity (P) of PR-CF and SM-CF Nanoparticles

sample	a (Å)	D (nm)	t (nm)	d_X (g/cm^3)	d_B (g/cm^3)	P (%)
PR-CF	8.355	9.64	9.5	5.336	3.633	33.53
SM-CF	8.362	10.40	10	5.364	3.668	31.83

The morphology of PR-CF and SM-CF analyzed by transmission electron microscopy (TEM), as shown in Figure 1, was found to be spherical in nature for both samples. The slight agglomeration of SM-CF is also attributed to the magnetic interaction among the nanoparticles, which results in the lowering of surface energy and depends on the communal performance of NPs and intermolecular force offered among them. The particle size (t) values determined from TEM data are found to be 9.5 and 10 nm for the PR-CF and SM-CF nanoparticles, respectively. These values well match with the crystallite size (D) values calculated from the XRD data. The SAED patterns of PR-CF and SM-CF are shown in Figure 1. The crystal planes of (111), (200), (311), and (400) were observed in both the SAED patterns. The SAED pattern of SM-CF confirmed the functionalization of oleic acid on the surface of PR-CF, which did not modify the crystal structure of the PR-CF. The brightness of the SAED pattern slightly decreased in the case of SM-CF, due to the amorphous nature of the oleic acid layer on the surface of $CoFe_2O_4$.

Thermogravimetric analysis (TGA) of PR-CF and SM-CF was studied to examine the phase development temperature of the spinel cubic structure. The TGA plot of PR-CF and SM-CF is shown in Figure 2. The curve shows the elimination of nitrates trailed by the development of the spinel ferrite phase with respect to temperature. The TGA curve demonstrates total weight losses of 21.18 and 24.87% for the PR-CF and SM-CF samples, respectively, as seen in Figure 2. Also, it is noted from the TGA curve that there is no notable weight loss beyond 450 °C, which is accredited to spinel ferrite phase development. The decomposition of the SM-CF sample started at 170 °C and ended at 440 °C with a total weight loss of 24.87%. This weight loss of 24.87% emerged from the disintegration of oleic acid, which is presented on the core of the SM-CF sample. This validates the total % of oleic acid as 24.87% on the SM-CF core.

The Fourier transform infrared (FT-IR) spectra of PR-CF and SM-CF are shown in Figure 2. The emergence of bands at 544 and 363 cm^{-1} corresponds to the stretching vibrations of Fe^{3+}−O_2 and Co, which appeared in both the PR-CF and SM-CF samples.[32,33] The peaks at about 3418 cm^{-1} are assigned to O−H vibrations. The peaks at 544 and 363 cm^{-1} are assigned to Fe at the tetrahedral location, whereas the peaks at 1068 and 845 cm^{-1} are due to the stretching vibration mode related to the C−O band. The peaks at 1628 and 1404 cm^{-1} are due to the asymmetric and symmetric stretching linked with the COO− band, respectively. The carboxylic acid groups are then present in a COO− conformation. The peak at 3026 cm^{-1} is due to the asymmetric stretching linked with the CH_2 band. This observation indicates the existence of carboxylic molecules on the nanoparticle surface, which also confirms the functionalization of the oleic acid layer over the cobalt ferrite nanoparticles. The obtained peaks are well matched with earlier reports.[34]

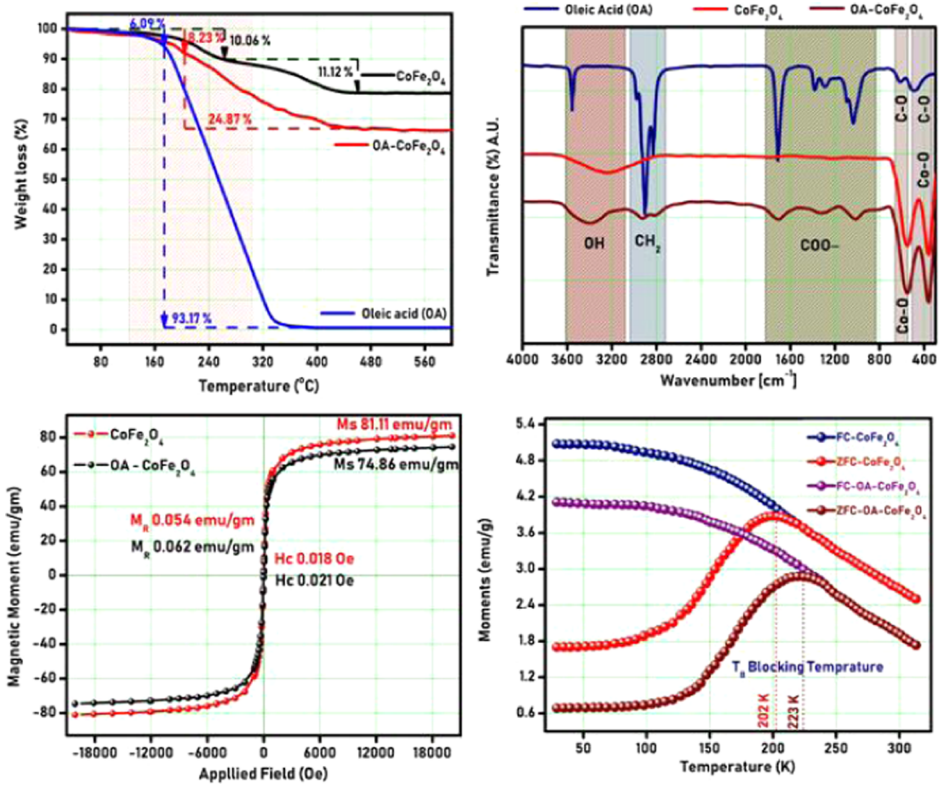

Figure 2. TGA plot, Fourier transform infrared (FT-IR) spectra, M−H plot, and field-cooled and zero-field-cooled (FC−ZFC) plot of PR-CF and SM-CF nanoparticles.

https://dx.doi.org/10.1021/acsomega.0c03332
ACS Omega 2020, 5, 23378−23384

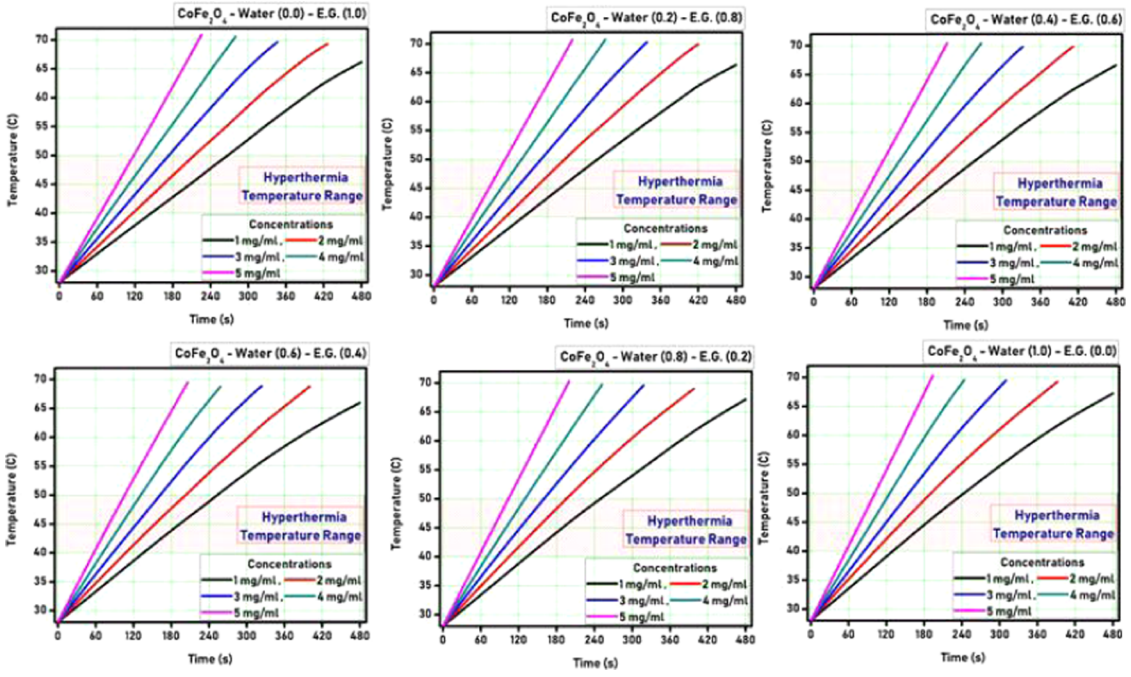

Figure 3. Hyperthermia curves for PR-CF nanoparticles.

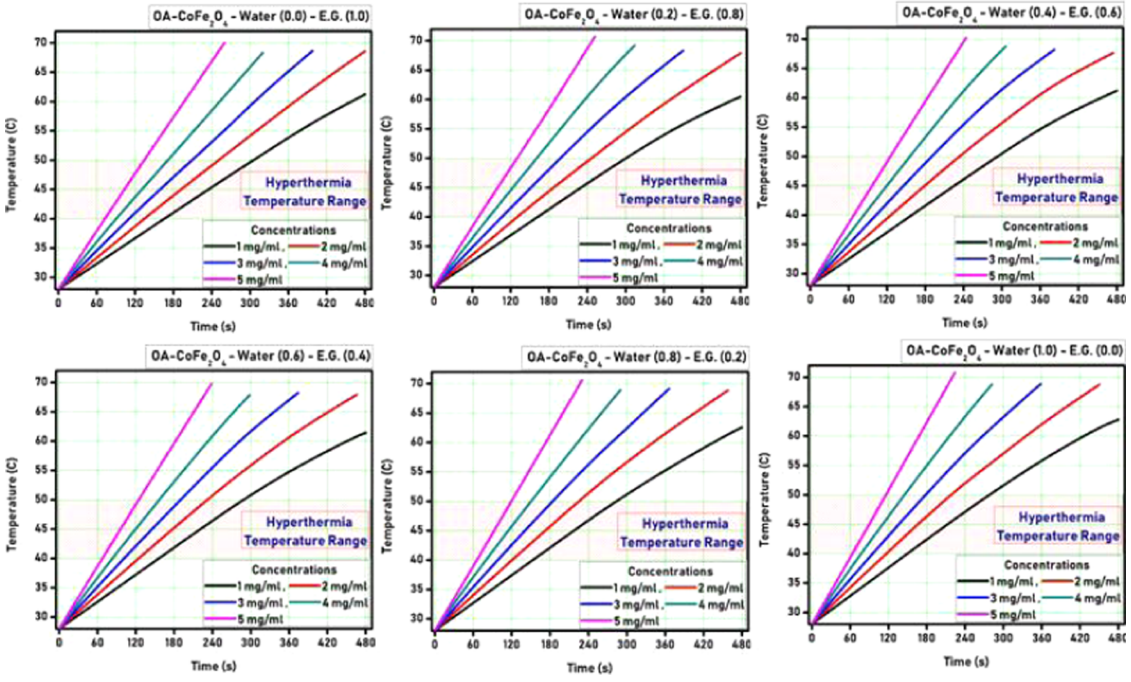

Figure 4. Hyperthermia curves for SM-CF nanoparticles.

The magnetic properties of PR-CF and SM-CF were studied by M−H plots with an applied field of ±21 kOe at 300 K, and the obtained results are shown in Figure 2. From Figure 2, it is revealed that the saturation magnetization (M_S) value of SM-CF (76.86 emu/g) is slightly less in comparison to M_S values of PR-CF (81.11 emu/g). The slight decrease in the M_S value for SM-CF is due to the oleic acid layer, which decreases the interparticle interface and the exchange coupling energy, which in turn reduces the magnetization. Both the PR-CF and SM-CF samples show very small and negligible values of remanent magnetism (M_R) and coercivity (H_C), which confirms the superparamagnetic nature of both the samples.[35] The decrease of the magnetization values can also be linked with the mass correction of the nonmagnetic oleic acid content covered on the core of the SM-CF sample. The mass correction can be evidenced by thermogravimetric analysis, which ensured 24.87% oleic acid content over the core of the SM-CF sample. The field-cooled and zero-field-cooled (FC−ZFC) plots of PR-CF and SM-CF are shown in Figure 2. The FC−ZFC plots show blocking temperature (T_B) of PR-CF and SM-CF. The ZFC curve reached the maximum at about 202 K for PR-CF and 223 K for SM-CF, which correspond to the blocking temperature

https://dx.doi.org/10.1021/acsomega.0c03332
ACS Omega 2020, 5, 23378−23384

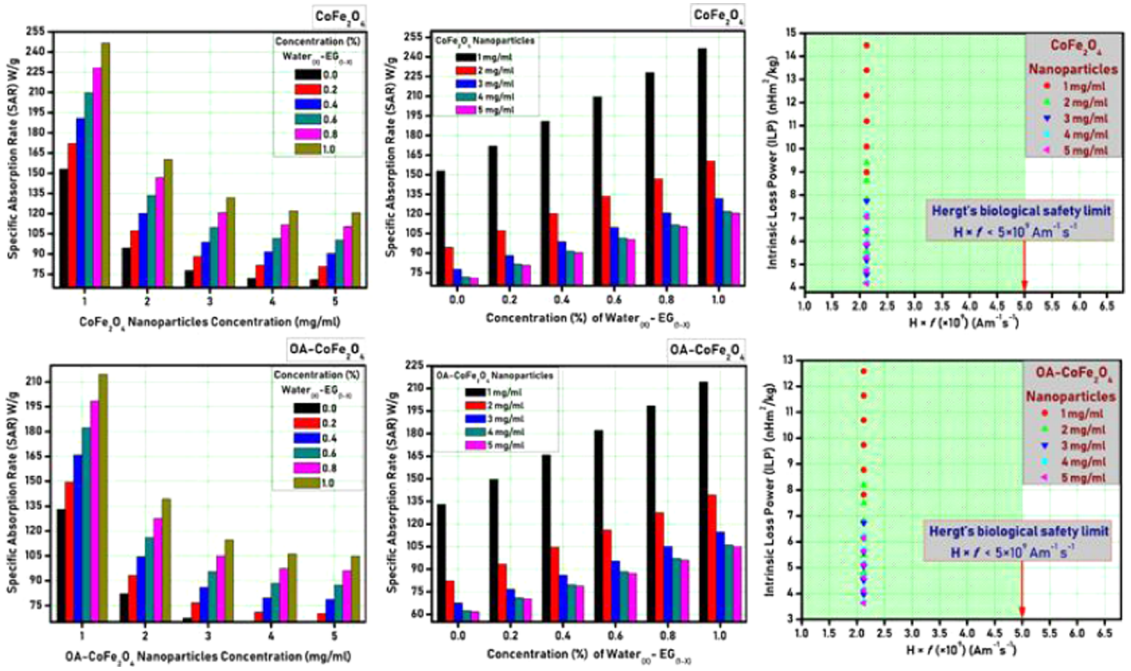

Figure 5. SAR and ILP plots for PR-CF and SM-CF nanoparticles.

(T_B) of the sample. Above T_B, the sample shows superparamagnetic behavior. The blocking temperature (T_B) of SM-CF was slightly greater compared to PR-CF, which is caused due to oleic acid functionalization.

The heat generation ability of both the PR-CF and SM-CF samples was tested using an induction heating system. Both the PR-CF and SM-CF samples were dispersed in ethylene glycol/water with various concentrations and characterized by the induction heating technique for evaluation of their self-heating characteristics. A series of temperature versus time measurements were done by varying the ethylene glycol/water (EG/W) proportion for better understanding of the self-heating characteristics of the prepared $CoFe_2O_4$ nanoparticles. Figures 3 and 4 show the hyperthermia curves for different nanoparticle concentrations as well as varying ethylene glycol/water proportions for PR-CF and SM-CF samples, respectively.

It is observed from Figures 3 and 4 that all of the curves show a gradual increase in temperature with respect to time. The time required for the temperature rise decreased with the increase of nanoparticle concentration for both the PR-CF and SM-CF samples. The hyperthermia temperature was achieved at 65 s by the PR-CF sample with 1 mg/mL concentration, whereas for 5 mg/mL concentration, it was 55 s. Similarly, the hyperthermia temperature range was achieved at 70 s by the SM-CF sample with 1 mg/mL concentration, whereas for 5 mg/mL concentration, it was 60 s. It is also observed from the curves that the increase in temperature was slightly decreased after the oleic acid coating over the $CoFe_2O_4$ nanoparticles. This slight decrease can be attributed to the decrease of saturation magnetization, which directly affects the heating ability of the nanoparticles.

Specific absorption rate (SAR) is one of the important parameters that plays a significant role in the application of MNPs in hyperthermia therapy. The following equation was used to calculate the SAR[36]

$$\text{specific absorption rate (SAR)} = C\frac{\Delta T}{\Delta t}\frac{1}{m_{Fe}}$$

Figure 5 shows the SAR plots for different nanoparticle concentrations as well as varying ethylene glycol/water proportion for PR-CF and SM-CF samples, respectively. It is observed from Figure 5 that the SAR value decreases with an increase in the nanoparticle concentration, whereas it increases with an increase in water concentration. The highest SAR values of the order of 248 W/g was observed for the PR-CF sample with 1 mg/mL concentration. This SAR value was decreased to 216 W/g for the SM-CF sample due to oleic acid coating. This shows that the SM-CF sample with 1 mg/mL concentration is sufficient to produce the required heat for hyperthermia treatment.

3. CONCLUSIONS

Oleic acid-coated $CoFe_2O_4$ nanoparticles were successfully synthesized using the chemical co-precipitation route. The Rietveld refined XRD pattern of $CoFe_2O_4$ nanoparticles indicated the formation of a cubic-spinel single-phase structure with the $Fd\bar{3}m$ space group. The average crystallite size (~12 nm) confirmed the nanocrystalline appearance of the prepared $CoFe_2O_4$ nanoparticles. TEM images revealed the spherical nature of both ($CoFe_2O_4$) and (OA-$CoFe_2O_4$) samples. The absorption bands in the FT-IR spectrum at ~3418, 3026, 1628, 1404, 1068, 845, 544, and 363 cm^{-1} affirmed the spinel ferrite formation and OA attachment. The M−H curve recorded at room temperature showed the superparamagnetic nature of the $CoFe_2O_4$ nanoparticles with moderate saturation magnetization (~78 emu/gm). The blocking temperature of the prepared $CoFe_2O_4$ nanoparticles obtained from the FC−ZFC curve was estimated to be 144 K. Oleic acid-coated $CoFe_2O_4$ nanoparticles with a minimum concentration (1 mg/mL) offers its potentiality in magnetic fluid hyperthermia toward noninvasive cancer treatment subject to the biocompatibility studies and consecutive clinical trials.

https://dx.doi.org/10.1021/acsomega.0c03332
ACS Omega 2020, 5, 23378−23384

4. EXPERIMENTAL SECTION

$CoFe_2O_4$ nanoparticles were synthesized by the chemical co-precipitation route. Nitrates of cobalt and iron were independently dissolved in a stoichiometric ratio of 1:2 to get the precursors. The pH of the mixed solution was noted as 3. The pH was then adjusted by adding 2 M NaOH. A black precipitate was obtained by heating the solution up to boiling temperature for 2 h. The obtained precipitate was washed several times with water. Furthermore, 2 M nitric acid (HNO_3) was added to the precipitate to eliminate impurities. The nanoparticles were filtered and dried at 55 °C for 24 h. The surface of the $CoFe_2O_4$ nanoparticles was modified with oleic acid by the ultrasonication process. The pristine and surface-modified $CoFe_2O_4$ samples were coded as PR-CF and SM-CF, respectively. The characterization techniques used in the current work are summarized in Table 2.

Table 2. Characterization Techniques Employed in the Current Work

characterization tool	make and model	specification
"XRD"	Make: Rigaku; model: Ultima IV	room temperature; 2θ range: 10−80°; λ = 1.540 Å; step size: 0.040°/76.80 s
"FT-IR"	Make: Thermo Scientific; model: Nicolet iS10	room temperature; wavenumber range: 300−4000 cm^{-1} resolution: 0.5 cm^{-1}
"TGA"	Make: Shimadzu; model: TGA-51	nitrogen atmosphere, room temperature to 600 °C;
"TEM"	Make: PHILIPS; model: CM-200	energy: 20−200 kV; resolution: 2.4 Å
"VSM"	Make: "Lakeshore" model: VSM 7407	room temperature and 5 K; Field: ±21 kOe
"induction heating"	Make: Ambrell model: Easy Heat 8310	field: 35 kA/m frequency: 350 kHz

AUTHOR INFORMATION

Corresponding Authors

Prashant B. Kharat − *Department of Physics, Dr. Babasaheb Ambedkar Marathwada University, Aurangabad 431004, Maharashtra, India; Department of Physics, Vinayak Vidnyan Mahavidyalaya, Amravati 444708, Maharashtra, India;* orcid.org/0000-0002-4187-2820; Email: drpbkharat@gmail.com

Sandeep B. Somvanshi − *Department of Physics, Dr. Babasaheb Ambedkar Marathwada University, Aurangabad 431004, Maharashtra, India;* orcid.org/0000-0003-2267-2724; Email: sbsomvanshi1993@gmail.com

Pankaj P. Khirade − *Department of Physics, Shri Shivaji Science College, Amravati 444603, Maharashtra, India*; Email: pankajkhirade@gmail.com

K. M. Jadhav − *Department of Physics, Dr. Babasaheb Ambedkar Marathwada University, Aurangabad 431004, Maharashtra, India*; Email: drjadhavkm@gmail.com

Complete contact information is available at: https://pubs.acs.org/10.1021/acsomega.0c03332

Notes

The authors declare no competing financial interest.

ACKNOWLEDGMENTS

P.B.K. acknowledges Dr. Raghumani S. Ningthoujam, Scientific Officer F, Bhabha Atomic Research Centre, Mumbai, for providing induction heating measurement facility. S.B.S. acknowledges Department of Science and Technology (DST), Govt. of India, for DST-INSPIRE Fellowship (IF170288).

REFERENCES

(1) Tran, N.; Webster, T. J. Magnetic nanoparticles: biomedical applications and challenges. *J. Mater. Chem.* **2010**, *20*, 8760−8767.

(2) Gao, J.; Gu, H.; Xu, B. Multifunctional magnetic nanoparticles: design, synthesis, and biomedical applications. *Acc. Chem. Res.* **2009**, *42*, 1097−1107.

(3) Hao, R.; Xing, R.; Xu, Z.; Hou, Y.; Gao, S.; Sun, S. Synthesis, functionalization, and biomedical applications of multifunctional magnetic nanoparticles. *Adv. Mater.* **2010**, *22*, 2729−2742.

(4) Berry, C. C. Possible exploitation of magnetic nanoparticle−cell interaction for biomedical applications. *J. Mater. Chem.* **2005**, *15*, 543−547.

(5) Somvanshi, S. B.; Kharat, P. B.; Saraf, T. S.; Somwanshi, S. B.; Shejul, S. B.; Jadhav, K. M. Multifunctional nano-magnetic particles assisted viral RNA-extraction protocol for potential detection of COVID-19. *Mater. Res. Innovations* **2020**, 1−6.

(6) Kale, S. B.; Somvanshi, S. B.; Sarnaik, M. N.; More, S. D.; Shukla, S. J.; Jadhav, K. M. Enhancement in surface area and magnetization of CoFe2O4 nanoparticles for targeted drug delivery application. *AIP Conf. Proc.* **2018**, *1953*, No. 030193.

(7) Périgo, E. A.; Hemery, G.; Sandre, O.; Ortega, D.; Garaio, E.; Plazaola, F.; Teran, F. J. Fundamentals and advances in magnetic hyperthermia. *Appl. Phys. Rev.* **2015**, *2*, No. 041302.

(8) Deatsch, A. E.; Evans, B. A. Heating efficiency in magnetic nanoparticle hyperthermia. *J. Magn. Magn. Mater.* **2014**, *354*, 163−172.

(9) Patade, S. R.; Andhare, D. D.; Somvanshi, S. B.; Jadhav, S. A.; Khedkar, M. V.; Jadhav, K. M. Self-heating evaluation of superparamagnetic MnFe2O4 nanoparticles for magnetic fluid hyperthermia application towards cancer treatment. *Ceram. Int.* **2020**, DOI: 10.1016/j.ceramint.2020.07.029.

(10) Patade, S. R.; Andhare, D. D.; Somvanshi, S. B.; Kharat, P. B.; More, S. D.; Jadhav, K. M. Preparation and characterisations of magnetic nanofluid of zinc ferrite for hyperthermia. *Nanomater. Energy* **2020**, 8−13.

(11) Martinez-Boubeta, C.; Simeonidis, K.; Makridis, A.; Angelakeris, M.; Iglesias, O.; Guardia, P.; Cabot, A.; Yedra, L.; Estradé, S.; Peiró, F.; et al. Learning from nature to improve the heat generation of iron-oxide nanoparticles for magnetic hyperthermia applications. *Sci. Rep.* **2013**, *3*, No. 1652.

(12) Thomas, L. A.; Dekker, L.; Kallumadil, M.; Southern, P.; Wilson, M.; Nair, S. P.; Pankhurst, Q. A.; Parkin, I. P. Carboxylic acid-stabilised iron oxide nanoparticles for use in magnetic hyperthermia. *J. Mater. Chem.* **2009**, *19*, 6529−6535.

(13) Blanco-Andujar, C.; Ortega, D.; Southern, P.; Pankhurst, Q.; Thanh, N. High performance multi-core iron oxide nanoparticles for magnetic hyperthermia: microwave synthesis, and the role of core-to-core interactions. *Nanoscale* **2015**, *7*, 1768−1775.

(14) Humbe, A. V.; Kounsalye, J. S.; Somvanshi, S. B.; Kumar, A.; Jadhav, K. M. Cation distribution, magnetic and hyperfine interaction studies of Ni−Zn spinel ferrites: role of Jahn Teller ion (Cu2+) substitution. *Mater. Adv.* **2020**, *1*, 880−890.

(15) Sanpo, N.; Berndt, C. C.; Wen, C.; Wang, J. New Approaches to the Study of Spinel Ferrite Nanoparticles for Biomedical Applications. In *Handbook of Nanoelectrochemistry: Electrochemical Synthesis Methods, Properties and Characterization Techniques*,Aliofkhazraei, M.; Makhlouf, A. S. H., Eds.; Springer International Publishing: Cham, 2016; pp 1−21.

(16) Tatarchuk, T.; Bououdina, M.; Vijaya, J. J.; Kennedy, L. J. In *Spinel Ferrite Nanoparticles: Synthesis, Crystal Structure, Properties, and Perspective Applications*, International Conference on Nanotechnology and Nanomaterials; Springer, 2016; pp 305−325.

(17) Amiri, M.; Salavati-Niasari, M.; Akbari, A. Magnetic nanocarriers: Evolution of spinel ferrites for medical applications. *Adv. Colloid Interface Sci.* **2019**, *265*, 29−44.
(18) Chavan, A. R.; Somvanshi, S. B.; Khirade, P. P.; Jadhav, K. M. Influence of trivalent Cr ion substitution on the physicochemical, optical, electrical, and dielectric properties of sprayed NiFe2O4 spinel-magnetic thin films. *RSC Adv.* **2020**, *10*, 25143−25154.
(19) Kharat, P. B.; Somvanshi, S. B.; Kounsalye, J. S.; Deshmukh, S. S.; Khirade, P. P.; Jadhav, K. M. Temperature dependent viscosity of cobalt ferrite/ethylene glycol ferrofluids. *AIP Conf. Proc.* **2018**, *1942*, No. 050044.
(20) Kharat, P. B.; More, S. D.; Somvanshi, S. B.; Jadhav, K. M. Exploration of thermoacoustics behavior of water based nickel ferrite nanofluids by ultrasonic velocity method. *J. Mater. Sci.: Mater. Electron.* **2019**, *30*, 6564−6574.
(21) Somvanshi, S. B.; Jadhav, S. A.; Khedkar, M. V.; Kharat, P. B.; More, S. D.; Jadhav, K. M. Structural, thermal, spectral, optical and surface analysis of rare earth metal ion (Gd3+) doped mixed Zn−Mg nano-spinel ferrites. *Ceram. Int.* **2020**, *46*, 13170−13179.
(22) Kardile, H. J.; Somvanshi, S. B.; Chavan, A. R.; Pandit, A. A.; Jadhav, K. M. Effect of Cd2+ doping on structural, morphological, optical, magnetic and wettability properties of nickel ferrite thin films. *Optik* **2020**, *207*, No. 164462.
(23) Jadhav, S. A.; Somvanshi, S. B.; Khedkar, M. V.; Patade, S. R.; Jadhav, K. M. Magneto-structural and photocatalytic behavior of mixed Ni−Zn nano-spinel ferrites: visible light-enabled active photodegradation of rhodamine B. *J. Mater. Sci.: Mater. Electron.* **2020**, *31*, 11352−11365.
(24) Borade, R. M.; Somvanshi, S. B.; Kale, S. B.; Pawar, R. P.; Jadhav, K. M. Spinel zinc ferrite nanoparticles: an active nanocatalyst for microwave irradiated solvent free synthesis of chalcones. *Mater. Res. Express* **2020**, *7*, No. 016116.
(25) Amiri, S.; Shokrollahi, H. The role of cobalt ferrite magnetic nanoparticles in medical science. *Mater. Sci. Eng., C* **2013**, *33*, 1−8.
(26) Somvanshi, S. B.; Patade, S. R.; Andhare, D. D.; Jadhav, S. A.; Khedkar, M. V.; Kharat, P. B.; Khirade, P. P.; Jadhav, K. M. Hyperthermic evaluation of oleic acid coated nano-spinel magnesium ferrite: Enhancement via hydrophobic-to-hydrophilic surface transformation. *J. Alloys Compd.* **2020**, *835*, No. 155422.
(27) Somvanshi, S. B.; Kumar, R. V.; Kounsalye, J. S.; Saraf, T. S.; Jadhav, K. M. Investigations of structural, magnetic and induction heating properties of surface functionalized zinc ferrite nanoparticles for hyperthermia applications. *AIP Conf. Proc.* **2019**, *2115*, No. 030522.
(28) Salunkhe, A.; Khot, V.; Thorat, N.; Phadatare, M.; Sathish, C.; Dhawale, D.; Pawar, S. Polyvinyl alcohol functionalized cobalt ferrite nanoparticles for biomedical applications. *Appl. Surf. Sci.* **2013**, *264*, 598−604.
(29) Baldi, G.; Bonacchi, D.; Franchini, M. C.; Gentili, D.; Lorenzi, G.; Ricci, A.; Ravagli, C. Synthesis and coating of cobalt ferrite nanoparticles: a first step toward the obtainment of new magnetic nanocarriers. *Langmuir* **2007**, *23*, 4026−4028.
(30) Andhare, D. D.; Patade, S. R.; Kounsalye, J. S.; Jadhav, K. M. Effect of Zn doping on structural, magnetic and optical properties of cobalt ferrite nanoparticles synthesized via. Co-precipitation method. *Phys. B* **2020**, *583*, No. 412051.
(31) Patade, S. R.; Andhare, D. D.; Kharat, P. B.; Humbe, A. V.; Jadhav, K. M. Impact of crystallites on enhancement of bandgap of Mn1-xZnxFe2O4 ($1 \geq x \geq 0$) nanospinels. *Chem. Phys. Lett.* **2020**, *745*, No. 137240.
(32) Somvanshi, S. B.; Khedkar, M. V.; Kharat, P. B.; Jadhav, K. M. Influential diamagnetic magnesium (Mg2+) ion substitution in nano-spinel zinc ferrite (ZnFe2O4): Thermal, structural, spectral, optical and physisorption analysis. *Ceram. Int.* **2020**, *46*, 8640−8650.
(33) Bharati, V. A.; Somvanshi, S. B.; Humbe, A. V.; Murumkar, V. D.; Sondur, V. V.; Jadhav, K. M. Influence of trivalent Al−Cr co-substitution on the structural, morphological and Mössbauer properties of nickel ferrite nanoparticles. *J. Alloys Compd.* **2020**, *821*, No. 153501.
(34) Somvanshi, S. B.; Kharat, P. B.; Khedkar, M. V.; Jadhav, K. M. Hydrophobic to hydrophilic surface transformation of nano-scale zinc ferrite via oleic acid coating: Magnetic hyperthermia study towards biomedical applications. *Ceram. Int.* **2020**, *46*, 7642−7653.
(35) Karaagac, O.; Bilir, B.; Kockar, H. Superparamagnetic cobalt ferrite nanoparticles: effect of temperature and base concentration. *J. Supercond. Novel Magn.* **2015**, *28*, 1021−1027.
(36) Lanier, O. L.; Korotych, O. I.; Monsalve, A. G.; Wable, D.; Savliwala, S.; Grooms, N. W.; Nacea, C.; Tuitt, O. R.; Dobson, J. Evaluation of magnetic nanoparticles for magnetic fluid hyperthermia. *Int. J. Hyperthermia* **2019**, *36*, 686−700.

https://dx.doi.org/10.1021/acsomega.0c03332
ACS Omega 2020, 5, 23378−23384